ELSEVIER

PII: S0032-3861(97)00595-8

Polymer Vol. 39 No. 13, pp. 2867–2874, 1998

0032-3861/98/$19.00+0.00

Phase separation in hexamethylenetetramine cross-linked Novolac/poly(ethylene-*co*-vinyl acetate) blends

Wenjie Chen*, Jian Wu and Ming Jiang
Department of Macromolecular Science and the Lab of Molecular Engineering of Polymer, Fudan University, Shanghai 200433, China
(Received 27 January 1997; revised 16 July 1997; accepted 4 August 1997)

Phase separation during curing reaction in the system of Novolac/poly(ethylene-*co*-vinyl acetate) (EVA) loaded with hexamethylenetetramine (Hexa) was investigated by time-resolved light scattering (TRLS), optical microscopy and scanning electron micrograph (SEM). Novolac/EVA mixtures showed a lower critical solution temperature (LCST) phase diagram with a high asymmetry in which the immiscible region emerges at high temperature and high Novolac contents. Hydrogen-bonding interaction between Novolac and EVA was verified by *FT*i.r. measurement as well. As the curing reaction proceeded, an initially homogeneous Novolac/EVA/Hexa mixture underwent phase separation via spinodal decomposition (SD), which was induced by depression of LCST with the increase of the molecular weight of Novolac. A regular and cocontinuous phase-separated structure was finally formed for the cured Novolac/EVA mixture. Time-resolved light scattering investigation showed that the process of SD during curing was different from that in ordinary thermally induced SD, i.e. q_m, the wavenumber q at the peak position of the scattering profile, increases with time in the early stage of curing. The structure formation process was discussed in terms of the SD mechanism based on the investigation of TRLS and SEM observation. The scaling structure functions analysis and SEM observation show that the final morphology of the cured mixture may be yielded through the route of the cluster to the cocontinuous structure.

(Keywords: spinodal decomposition; curing reaction; phenol-formaldehyde resin)

INTRODUCTION

The well-known Novolac, which is a typical phenol-formaldehyde resin, has found broad applications, such as in moulded parts, insulating and decorative varnished, laminated sheets, and cast products. Efforts have been made to improve the mechanical properties of phenol-formaldehyde resin by blending it with other polymers [1]. As most modified phenol-formaldehyde resins are utilized in a cured form, deeper understanding of the structure formation in the curing mixtures is of great importance in the development, optimization and properties-control of the systems.

Recently, the phase separation associated with reactions has been extensively studied (see, for example, [2]). It has been well-established that, in the cases of multicomponent thermoset resins such as epoxy/poly(ether sulphone) [3] and epoxy/liquid rubber systems [4,5], and higher impact strength acrylics such as methyl methacrylate/poly(ethylene-*co*-vinyl acetate) (EVA) system [6], phase separation took place via spinodal decomposition (SD) induced by reactions, and the phase structure development could be interpreted in terms of the structure formation mechanism via SD. Depending on the relative rate of phase separation and reaction, spinodal decomposition induced by reactions yielded a variety of regular morphologies: such as interconnected globule structure, bimodal domain structure and isolated dispersed domain structure. The materials yielded by spinodal decomposition induced by reactions have been shown to exhibit excellent properties [2–5].

However, there have been few reports concerning SD in the curing Novolac resin modified with other polymers so far. Nakamura *et al.* studied the phase separation in curing the mixture of substituted phenol with various thermoplastic polymers in the presence of hexamethylenetetramine (Hexa) and they found that phase separation occurred via SD as well [7]. In this paper, we present our experimental results on phase separation during curing reaction in the system of Novolac/EVA blends loaded with Hexa. Novolac/EVA is expected to be miscible with a lower critical solution temperature (LCST) phase behaviour due to intermolecular hydrogen bonding between the hydroxyl groups in Novolac and carbonyl groups in EVA. When Novolac reacts with Hexa, a crosslinked structure can be formed leading to an increase in the molecular weight of Novolac and a consequent decrease in the combinatorial entropy. That results in the reduction of the miscibility. If the miscibility's reduction is sufficient to thrust the initial miscible blend into a two-phase regime in the phase diagram, phase separation will occur, assuming sufficient mobility and favourable kinetics. Thus, we may also expect SD induced by the curing reaction in the present system.

It is worth noting that, to our knowledge, although some studies have described the crosslinking effect on the miscibility of Novolac blends with intermolecular hydrogen bonding as a dominant driving force for the miscibility [8,9], no experimental observations of phase separation (macro-phase separation) during curing have been reported. For

* To whom correspondence should be addressed

example, the effect of crosslinking on the degree of molecular level mixing in the system of Novolac/EVA with Hexa was studied by Coleman and co-workers using Fourier transform infrared spectroscopy (*FT*i.r.). They suggested that the crosslinked blends were partial phase separation. However, insufficient evidence about the phase separation and the phase structures was given in the report [8]. Zhang *et al.* studied the phase structure of Hexa crosslinked Novolac/poly(methyl methacrylate) blends by high-resolution solid-state n.m.r. and differential scanning calorimetry (d.s.c.). They only found that the cured blends were partially miscible or microphase-separated with domain sizes around a scale of 20–30 nm [9].

In this study, our attention is focused on SD during curing in the present system. We first examined the phase diagram of Novolac/EVA blends as well as the hydrogen bonding interaction between the components by *FT*i.r., then we investigated the phase separation during curing the initially miscible Novolac/EVA mixture by time-resolved light scattering (TRLS). The two-phase structure in the cured system was observed by optical microscopy (OM). The formation of phase-separated structure was discussed based on the investigation above. We hoped that these results would aid in designing high-performance materials by control of the structure in Novolac resin modified with other polymers.

EXPERIMENTAL

Poly(ethylene-*co*-vinyl acetate) (EVA), purchased from Bayer Co., containing 50 wt% vinyl acetate, has a glass transition temperature of around 10°C, and number-average molecular weight of 7.0×10^4 g mol^{-1}. The Novolac resin was prepared by polymerization of phenol (containing 15 wt% Bisphenol-A of phenol) and formaldehyde (1 : 0.8 mol : mol ratio) with hydrochloric acid as catalyst (0.1 wt% of phenol), then the resin was separated, dried and pulverized. The number-average molecular weight and the glass transition temperature of Novolac resin are about 5×10^2 g mol^{-1} and 49.0°C, respectively. Hexamethylene-tetramine (Hexa), used as a curing agent of Novolac, was a commercial product without further purification.

Novolac resin was dried at 80°C under vacuum for 1 day before used. The film specimens of Novolac/EVA blends for optical microscopy observation were obtained as follows: homogeneous tetrahydrofuran (THF) solutions containing 4 wt% polymer in total were first prepared, the solvent was evaporated in a cover glass at about 30°C and following by further drying at 60°C under vacuum for more than 3 days. The film is about 30 μm thick.

The phase diagram of Novolac/EVA blends was obtained from OM observation. After the blend films on the cover glass were annealed at a given temperature for 24 h, some films became translucent and a phase separated structure was observed under OM, we judged that the blend was in the two-phase region in the phase diagram. Since some samples were still transparent and no indication of phase separation was seen under OM, we judged that the blend was in the single-phase region. The single-phase nature was carefully confirmed by further annealing at the same temperature for 48 h. These annealing experiments were repeated at various isothermal settings.

Fourier transform infrared spectroscopy measurements were performed with a Nicolet Magna-550 model spectrometer on all blends of Novolac/EVA in various proportions. Thin films were prepared by a similar procedure to that mentioned above, but casting on a KBr tablet. All films were sufficiently thin to ensure that the absorbance is in the range where the Beer–Lambert law is obeyed. The thickness of the samples was approximately constant.

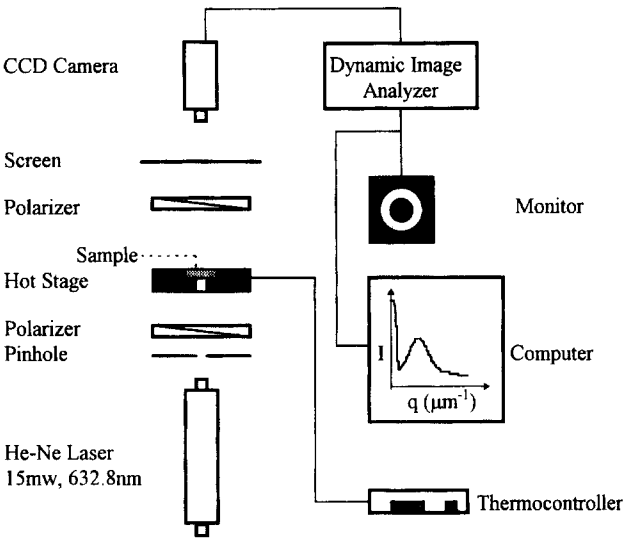

Figure 1 Experimental set-up of the time-resolved light-scattering apparatus

We also prepared solution-cast film of the mixture loaded with Hexa in 9/1 (v/v) CH_2Cl_2/THF mixture via a similar manner. Light-scattering measurements during curing were conducted on our homemade TRLS apparatus. The principle of apparatus was described in some earlier papers [10]. Here we only mentioned the parts relevant to the present study. *Figure 1* shows the set-up of our TRLS apparatus. The light source is a 15 mW plane-polarized He–Ne laser with a wavelength of 632.8 nm. The sample sandwiched between two cover glasses was inserted into a heating chamber kept at a constant temperature with an accuracy of $\pm$ 0.1°C. The chamber was set horizontally on the light-scattering stage as in *Figure 1*. Radiation from the He–Ne gas laser was applied vertically to the specimen. The scattered light intensity distribution $I(q)$ under a Vv (parallel polarized) optical alignment was determined using a two-dimensional CCD-camera detector with 512 $\times$ 512 pixels and an intensity resolution of 256 levels. The scattering vector $\mathbf{q}$ is related to the scattering angle θ and the wavelength λ of the laser in the sample,

$$q = (4\pi/\lambda)\sin(\theta/2) \quad (1)$$

The change in the light scattering profile was recorded at appropriate time intervals during isothermal annealing (curing). The measurements of Novolac/EVA 50/50 wt/wt with 15 wt% Hexa at 150°C were performed.

The cure reaction kinetics of Novolac/EVA/Hexa blend at 150°C was conducted by DSC (Shimadzu7A-50I). The conversion (degree of reaction) of mixtures was estimated by the area of the exothermic peak (temperature range 121~172°C) evolving from the reaction during the DSC heating run at 20°C min^{-1} as given by:

$$\text{conversion} = (1 - A_t/A_0) \times 100\% \quad (2)$$

where A_0 is the area of the exothermic peak of uncured material and A_t is that of material cured for a time t.

The change in the relative modulus of Novolac/EVA/Hexa mixture with curing time at 150°C was measured by a torsion pendulum analyser.

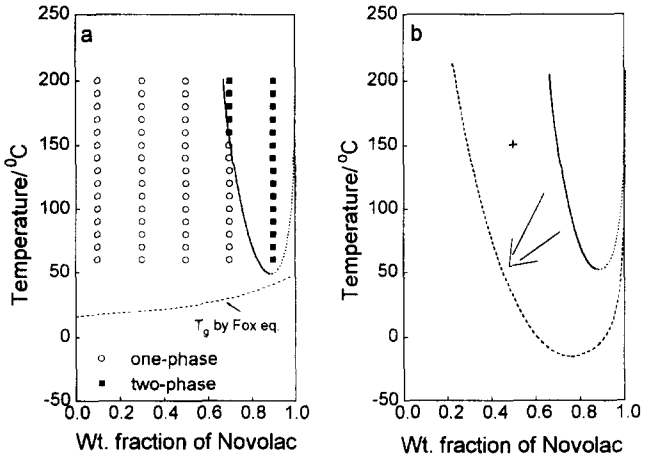

Figure 2 (a) Phase diagram for the Novolac/EVA blends. (b) Schematic representation for the variation of phase diagram with curing

The two-phase morphology of the specimens during curing reaction was observed using SEM (Hitachi HU-11B). After a sample was cured for a desired period, it was taken out and rapidly quenched to room temperature to fix the morphological structure of the sample. Then the sample was fractured in liquid N_2 and etched in CH_2Cl_2, which is a good solvent for EVA and a poor solvent for Novolac. Hence, EVA can be considered to be rinsed away. The etched surface was observed by SEM.

RESULTS AND DISCUSSION

Phase diagram of Novolac/EVA blends

The films of the binary mixtures of Novolac/EVA after being dried at 60°C under vacuum were transparent and homogeneous under the optical microscope with different compositions except 90/10 (wt/wt). The clarity was maintained even after annealing for 24 h over the entire experimental temperature range studied but 70/30 (wt/wt) Novolac/EVA mixture differed, i.e. after 24 h annealing at temperatures above 150°C, the mixture became translucent and a phase-separated structure was observed under a microscope. A 90/10 Novolac/EVA mixture remained opaque and a phase-separated structure was observed under a microscope over the whole temperature range. The single-phase nature of the mixture was carefully confirmed by further annealing for 24 h. On the basis of these observation, the boundary between one-phase and two-phase region was drawn in *Figure 2a*, showing an LCST-type phase diagram. The phase diagram shows obvious asymmetry in which the region of immiscibility

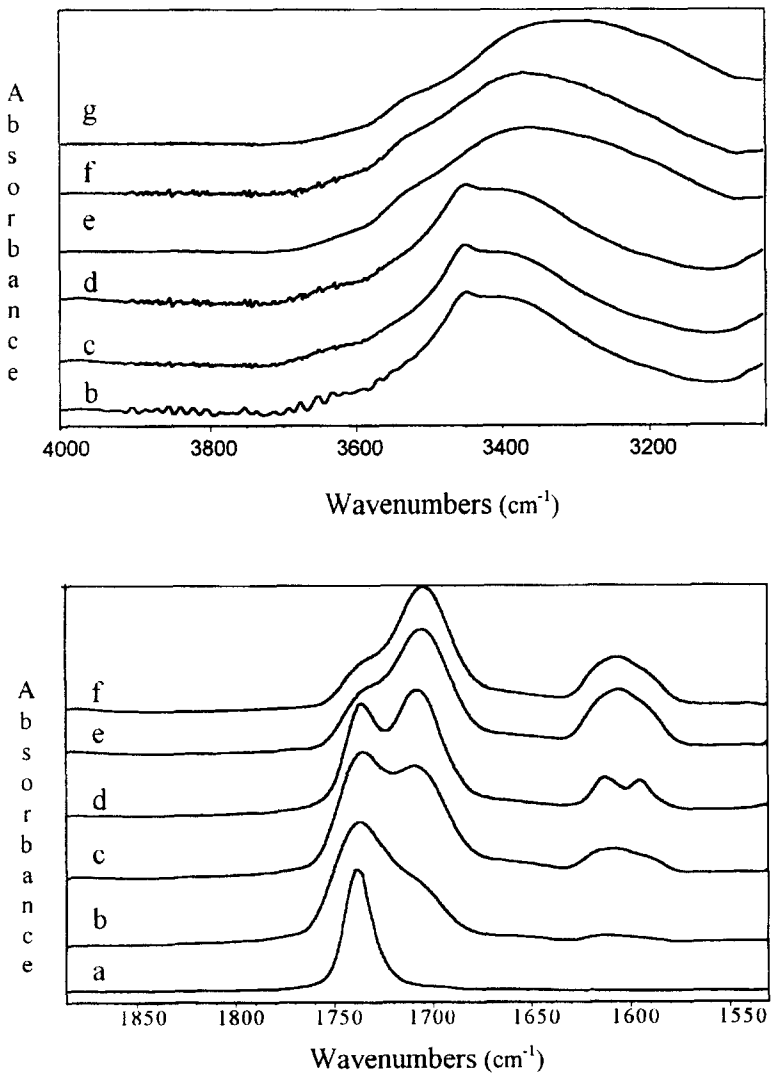

Figure 3 *FT*i.r. spectra in the hydroxyl stretching (top) and the carbonyl stretching (bottom) regions of the Novolac/EVA blends observed at 25°C. Novolac/EVA (w/w): (a) 0/100, (b) 10/90, (c) 30/70, (d) 50/50, (e) 70/30, (f) 90/10, (g) 100/0

emerges at high Novolac compositions. *Figure 2a* also shows the glass transition temperature (T_g) curve, estimated by the Fox equation using d.s.c. data of pure Novolac and EVA.

The miscibility of Novolac/EVA in wide composition and temperature ranges can be attributed to the hydrogen-bonding interaction between the carbonyl groups of EVA and the phenolic hydroxyl groups of Novolac. *Figure 3* shows the *FT*i.r. spectra in the hydroxyl stretching (top) and carbonyl stretching (bottom) regions of Novolac/EVA blends of various compositions at room temperature. Pure EVA is characteristic of free carbonyl stretching vibration at 1739 cm^{-1}. In the presence of Novolac in blends, the band of the carbonyl is split to form a doublet containing the absorption remaining at the higher frequency of free carbonyl and a new absorption peak at 1707 cm^{-1} associated with hydrogen-bonded carbonyl groups. The absorptions by hydrogen-bonded and 'free' carbonyl groups are enhanced and suppressed, respectively, with the increase in Novolac contents in blends.

Pure Novolac is characterized by a very broad band centred at 3300 cm^{-1}, attributed to wide distribution of hydrogen-bonded (self-associated) hydroxyl groups, and a much narrower band at 3525 cm^{-1}, which is associated with 'free' (non-hydrogen-bonded) phenolic hydroxyl groups. As seen in *Figure 3* (top), as the concentration of EVA is increased in the blends, the free hydroxyl band is reduced and is not evident in the 50/50, 30/70, 10/90 Novolac/EVA blends. Concurrently, the frequency maximum of the hydrogen-bonded (self-associated) hydroxyl band increases from about 3300 to ~3360 cm^{-1}, and an additional band in the spectra at 3450 cm^{-1} can be observed in the 50/50, 30/70, 10/90 Novolac/EVA blends, which is attributable to hydroxyl groups hydrogen-bonded to carbonyl groups. This result indicates that there was appreciable mixing at the molecular level in Novolac/EVA blends, which is in agreement with the result shown in the phase diagram (*Figure 2a*).

Unlike the carbonyl stretching regions of the *FT*i.r. spectrum, where there are only two bands attributed to 'free' and 'hydrogen-bonded' carbonyl groups, in the hydroxyl stretching region there are (at least) three major contributors, and the variation of the fraction of the 'free' and two different hydrogen-bonded hydroxyl groups as a function of blend composition is rather complex. While a quantitative calculation of the fraction of the different species is feasible in the carbonyl stretching region, quantitative analysis of the self-associating hydrogen bonds between Novolac is unfortunately impractical, because of the lack of reliable absorptivity coefficients and other complications.

Quantitative determination of the fraction of hydrogen-bonded carbonyl groups at room temperature was obtained from a least-squares fit of two Lorentz bands to the carbonyl stretching absorptions. *Figure 4* shows the resultant fraction of hydrogen-bonded carbonyl groups in Novolac/EVA blends as a function of composition of blends. In calculating the fraction of hydrogen-bonded carbonyl groups, band areas were connected for the absorption coefficient differences by applying the ratio, $a_{hb}/a_f = 1.5$ [11], where a_{hb} and a_f represent the absorption coefficients of the hydrogen-bonded and 'free' carbonyl bands, respectively. The fraction of hydrogen-bonded carbonyl groups increases as the contents of Novolac increases in the blends. The fraction of hydrogen-bonded carbonyl groups shows a maximum of about 0.8 in the blend of 90/10 Novolac/EVA, which means most of carbonyl groups of EVA can form

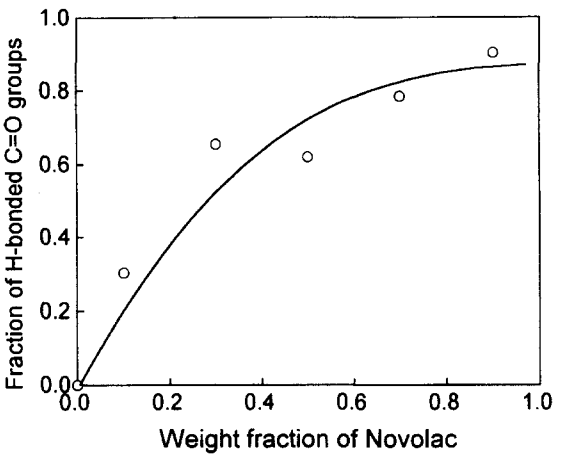

Figure 4 The fractions of hydrogen-bonded carbonyl groups as a function of the weight fraction of Novolac for Novolac/EVA blends

hydrogen-bonding with the phenolic hydroxyl groups of Novolac even though 90/10 Novolac/EVA blend is phase-separated at room temperature. This result may imply that the mixture consists of two coexisting phases, one of which is almost pure Novolac and the other composed of the two components, between which most of carbonyl in EVA is hydrogen-bonded with hydroxyl groups of Novolac.

The skewness of the phase diagram toward high Novolac composition in this system may be caused by the balance between the inter-associating and self-associating hydrogen bonds. With the increase of Novolac composition, the inter-associating hydrogen bonds between the carbonyl groups of EVA and the phenolic hydroxyl groups of Novolac increase, and the self-associating hydrogen bonds between the phenolic hydroxyl groups of Novolac increase as well. The immiscible region emerges at high Novolac composition may be the result of the latter prevailing over the former. This skewness is also observed by other experimental phase diagram on similar hydrogen-bonded polymer blends [12–14].

Phase separation during the curing reaction

For studying the phase separation during the curing reaction, we concentrated on Novolac/EVA/Hexa 50/50/15 curing at 150°C. This mixture is initially a single-phase system at curing temperature as can be seen from *Figure 2a*, assuming that the effect of the incorporation of Hexa on the miscibility can be neglected. When the curing reaction proceeds, Novolac increases in average molecular weight, branches, and crosslinks. While this is occurring, the two-phase region in the phase diagram increases in size and the LCST line falls, and the mixture is thrust into a two-phase regime. These situations are schematically demonstrated in *Figure 2b* (the mixture is indicated by a cross in *Figure 2b*). Hence spinodal decomposition is expected to take place in the curing process.

The time-resolved light-scattering profiles of Novolac/EVA/hexa 50/50/15 (wt) mixture curing at 150°C is shown in *Figure 5*. In the early stage of curing reaction, no appreciable scattered-light was observed, indicating a homogeneous mixture. A peak in the light-scattering profile appeared with a time lag, and then the intensity increased continuously with time. Note that the peak position shifts towards a larger angle as the curing reaction proceeds. This behaviour is very different from that observed in ordinary spinodal decomposition in the absence of reaction, and will

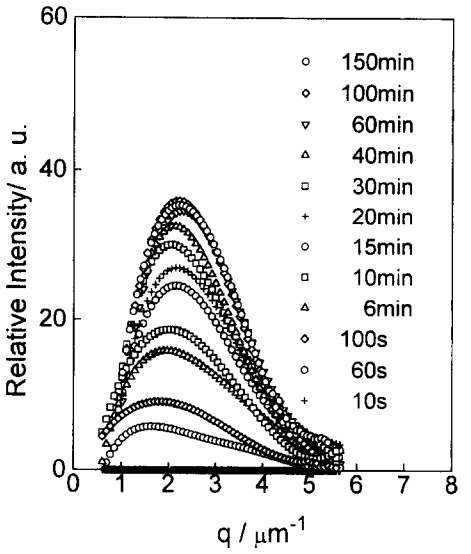

Figure 5 Time-variation of light scattering profiles during curing reaction for 50/50/15 (wt) Novolac/EVA/Hexa mixture at 150°C

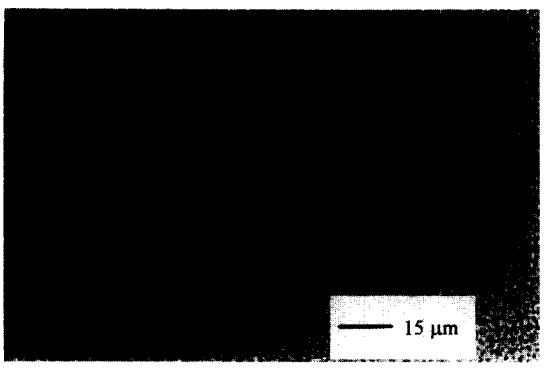

Figure 6 Optical micrograph for 50/50/15 (wt) Novolac/EVA/Hexa mixture cured at 150°C for 1 h

be discussed later in this paper. The scattering profiles became invariant after about 60 min. The peak formation in light-scattering profiles indicates the development of a regularly phase-separated structure with the periodic distance of $\Lambda_m = 2\pi/q_m$, q_m is the value of q at the peak. *Figure 6* shows the optical micrograph of the same specimen after curing for 1 h. The micrograph clearly shows the regular morphology with a periodic distance of about 2.5 μm and dual connectivity of phase. The characteristics of the morphology shown in *Figure 6* and the formation of peak in the light-scattering profiles are quite similar in appearance to that in the ordinary thermally induced SD. Hence, the resultant morphology after curing with the regular structure shown in *Figure 6* is developed by SD during the curing reaction.

Structure formation during the curing reaction

In *Figure 7*, q_m, the value of q at peak position, is plotted as a function of time t on a double logarithmic scale. I_m, the intensity at q_m, is similarly plotted in *Figure 7*. Both q_m and I_m increase with time in the early stage of curing. The time variation of q_m levels off at about 20 min, suggesting that further changing of the periodic distance between the coexisting two-phase structure is suppressed. However, I_m continues to increase with time slightly later than 20 min and eventually levels off at about 60 min, suggesting that

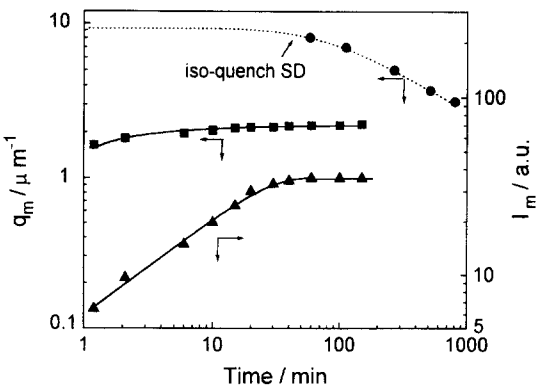

Figure 7 Time-dependence of q_m and I_m for 50/50/15 (wt) Novolac/EVA/Hexa mixture cured at 150°C in log–log plot. (Curve (··●··) indicates the time-dependence of q_m in the ordinary iso-quench thermally induced spinodal decomposition for polystyrene/poly(vinyl methyl ether) at 101°C [15]

the increase in composition difference between the coexisting two-phase proceeds further even after the dimension of phase-separated structure is fixed. In *Figure 7* we show a typical time dependence of q_m in ordinary thermally induced SD [15] as well. In ordinary iso-quench thermally induced SD, q_m initially appears at a high value and the peak position remains virtually invariant in the early stage. The growth of scattering intensity can be described with an exponential function of time predicted by the linearized theory of Cahn–Hilliard in this period [16], at a late time, q_m shifts to a lower value owing to the coarsening of the phase-separated structure to minimize its free energy by minimizing its interfacial area, and meanwhile the periodic distance increases with the coarsening, the dynamics of the coarsening process is found to be characterized by a power law [17]. Here it should be noted that the time-dependence of q_m between iso-quench SD and the present system cannot be directly compared on the values because of the different system; however, the differences in the characteristics of the phase separation process may be seen.

The increase in q_m with time observed in the early stage of curing reaction in Novolac/EVA/Hexa implies that the coarsening to a longer interdomain spacing is completely suppressed with the reaction. This suppression of the coarsening can be attributed to the successive increase in the quench depth during curing, that has been declared in the previous paper [18]. A similar phase-separation process was also observed in the curing reaction of epoxy/CTBN/DDM [5]. The qualitative interpretation of the coarsening suppression phenomenon is as follows. During the curing reaction, the quench depth ε is increased with the time as the consequence of continuously depressed down of the LCST lines. Here, quench depth ε is defined as

$$\varepsilon = |T - T_c| \tag{3}$$

to characterize the thermodynamic driving force for SD, where T and T_c are the temperatures of the phase separation and the critical point (in this case, the spinodal point), respectively. In the context of Cahn's theory, the wavenumber q_m of the dominant concentration fluctuation developed initially under a certain quench depth has the relation as [18]:

$$q_m = ((-\partial^2 f/\partial c^2)/4\kappa)^{1/2} \tag{4}$$

where f is the mean field free energy of mixing, κ is the gradient energy coefficient, and c is the volume fraction of one component of mixture. Even though equation (4) is

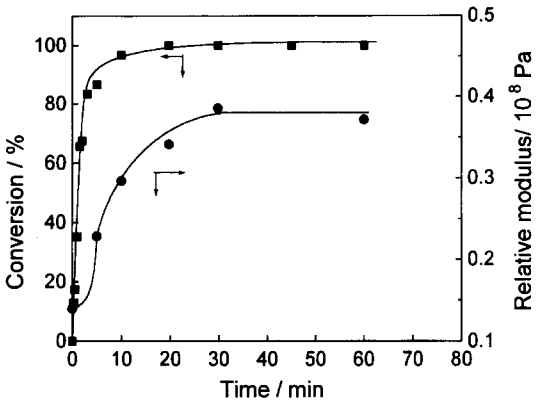

Figure 8 Time variation of conversion and relative modulus for 50/50/15 (wt) Novolac/EVA/Hexa mixture cured at 150°C

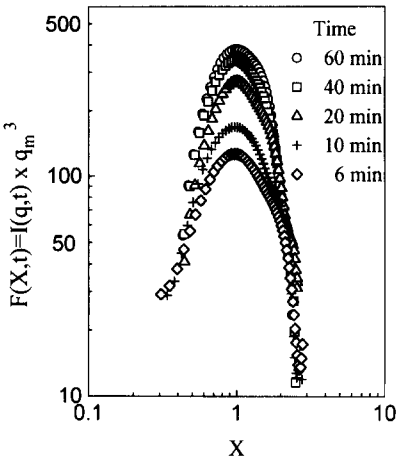

Figure 9 Time variation of scaled structure function $F(X, t)$ for 50/50/15 (wt) Novolac/EVA/Hexa mixture cured at 150°C

only available in the very early stage of SD, we may employ it to understand qualitatively the effects of successive increase in quench depth on the phase separation. Since the absolute value of $(-\partial^2 f/\partial^2 c)$ becomes larger as the quench depth increases, q_m is expected to increase with the increasing quench depth for a fixed κ. Thus, in the system of reaction-induced spinodal decomposition there is competition between two factors, i.e. the increase in quench depth resulting in an increase in q_m and the coarsening of phase-separated structure to minimizing the free energy by minimizing the interfacial area leading to the decrease in q_m. The complete suppression of the coarsening shown in the system studied here may be the result of the former prevailing over the latter, owing to the curing being faster compared with the phase separation [18]. If the curing reaction is fast enough, a new concentration fluctuation with a larger q_m (due to larger quench depth) may produce and overlap with the previous one, thereby the coarsening is suppressed and q_m increases with time.

The image of the morphology change corresponding to the increase in q_m with time may be described as follows. When the curing reaction proceeds, the compositions in the previously formed phase regions deviate from the coexisting values and become supersaturated; consequently, a new phase separation with a shorter periodic distance may take place within the each region of the two phases previously formed. The new phase structure may overlap with the previous one and that induced the increase of q_m with time (the reciprocal of q_m is proportional to the periodic distance or interparticle distance).

In *Figure 8*, both conversion and the relative modulus of cured mixtures are plotted against time. It clearly shows that the curing reaction proceeds very fast initially, which may interpret the increase in q_m with time in this period. The conversion arrives at ~80% at about 2 min, and then slows down and eventually levels off at about 20 min. The relative modulus of cured materials increases continuously with the curing time and then levels off at about 30 min. The onset of the increase in modulus with time is hard to determine from this time variation of the relative modulus, mainly owing to the fast reaction, which may make the onset of gelation occur at a short time (~5 min). Thus, the slowing down of the curing reaction after 5 min may be attributed to the gelation. After gelation, the diffusion of reactive components molecules in the network is retarded to a large extent. The increase in q_m with time in the early stage is also reduced after 5 min, which may be referred to the gelation as well.

The change of the characteristic of the phase-separated structure during curing reaction can be analysed based on the time evolution of the scaled structure function, which can be obtained from the time evolution of scattering profiles. Time evolution of a scattering profile $I(q, t)$ is expressed by [19]

$$I(q, t) \sim < \eta^2 > q_{m(t)}^{-3} S\left(\frac{q_{(t)}}{q_{m(t)}}\right) \quad (5)$$

where $S(q_{(t)}/q_{m(t)})$ is the structure function, and $< \eta^2 >$ is the mean-square fluctuation for the spatial variation of scattering contrast. Then the experimental scaled structure functions obtained by

$$F(X, t) = q_m(t)^3 I(q, t) \quad (6)$$

with $X = q(t)/q_m(t)$. From equation (5) and equation (6), $F(X, t)$ is related to $S(X)$ by

$$F(X, t) \sim < \eta^2 > S(X) \quad (7)$$

Furukawa [20] proposed the scaled structure function as

$$S(X) \propto \frac{X^2}{2+X^6} \text{ for cluster structure} \quad (8)$$

$$S(X) \propto \frac{X^2}{3+X^8} \text{ for cocontinuous percolated networks} \quad (9)$$

Figure 9 shows the time variation of $F(X, t)$ by double logarithmic plots calculated from the data in *Figure 5*. Up to 60 min, the intensity of $F(X, t)$ increases continuously with time, suggesting that the composition difference between the coexisting two-phase increases continuously even after the gelation. Meanwhile, the shape of the scaled structure function $F(X, t)$ varies with time as well, suggesting that the phase structure cannot be scaled with a universal structure function and the characteristic of the phase structure changes with curing reaction.

Figure 10 shows the double logarithmic plots of the reduced scaled structure $F(X, t)/F(1, t)$ at 20 min and 60 min, respectively. Note that the scaled structure functions in the X range $X > 1.6$ are obviously different, i.e. $F(X, t)$ in $1.6 < X < 2$ can be approximated by $F(X, t) \sim X^{-4}$ for $t = 20$ min, whereas $F(X, t) \sim X^{-6}$ for $t = 60$ min. According to equation (8) and equation (9), this change in power law of $F(X, t)$ may suggest that a cluster structure is formed after

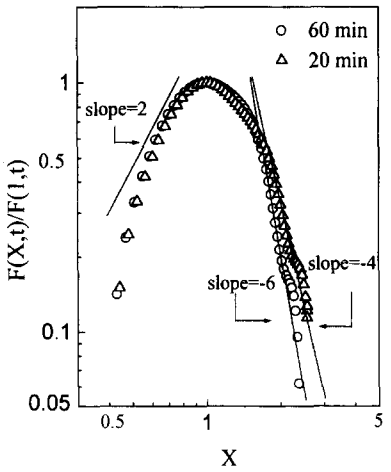

Figure 10 Reduced scaled structure function $F(X, t)/F(1, t)$ at $t = 20$ min and $t = 60$ min, respectively, for 50/50/15 (wt) Novolac/EVA/Hexa cured at 150°C

about 20 min of this SD process and then is changed to the cocontinuous percolated structure with the curing reaction. Such a morphological change during curing reaction has been proposed to explain the mechanism of the formation of the connected-globule structure of epoxy resin by Inoue *et al.* [2–5] and has been observed directly by Okada *et al.* [21] in the system of polystyrene/2-clorostyrene using SEM. The morphological change from clusters to cocontinuous is in the opposite direction compared with that during ordinary thermally induced spinodal decomposition in the absence of reaction, in which the cocontinuous structures formed initially break into clusters in the late stage. However, the results obtained from the analysis of time evolution of scaled structure function in our case may give new evidence to support the mechanism of structure development during SD induced by reaction proposed by Inoue *et al.* [2–5], i.e. the final cocontinuous phase structure may form through the route of cluster structure to cocontinuous structure.

Morphology by SEM

Figure 11 shows the structure development during phase separation for various times observed by SEM. Composition of Novolac/EVA/Hexa mixture and curing condition are the same as in *Figure 5*. As described before, these micrographs are obtained by SEM observation of the fractured and etched surfaces. Hence, EVA is rinsed away and the remaining material is a crosslinked Novolac-rich phase. The Novolac-rich phase formed clusters structure as seen in *Figure 11a* ($t = 20$ min). At $t = 40$ min (*Figure 11b*), it was observed that the clusters become connected to each other, and the total volume of clusters seems larger than that at $t = 20$ min, suggesting new regions of Novolac-rich phases are yielded with time. Finally, a non-spherical cocontinuous structure is observed clearly in *Figure 11c* ($t = 60$ min). Hence, the morphological structure development during reaction revealed by SEM observation is in agreement with the results predicted by the analyses of scaled structure function (*Figure 10*).

Based on the results shown in *Figures 5–11*, the structure formation process during curing of the Novolac/EVA mixture may be described as follows. Phase separation induced by the curing reaction took place via spinodal decomposition. A regularly phase-separated structure with a larger periodic distance was developed initially (it is suspected that the cluster phase structure was formed initially because the phase separation always occurs at an off-critical composition; however, it is not certain), and a cluster phase structure was shown to be formed in the intermediate stage of this SD process. The periodic distance of phase-separated structure gradually decreased as curing proceeded, suggesting that the phase separation may take place as well within the regions of two phases previously formed to form a new generation of clusters rather than the coalescence of cluster structure. Meanwhile, the composition difference between the coexisting two phases increased rapidly with time. After gelation the composition difference between the coexisting two-phase grows continuously, but the rate of increase in composition difference was reduced because the mobility of the component molecules decreased. The clusters finally contacted with each other resulting in the cocontinuous structure with a periodic nature. Eventually, the composition difference between coexisting two-phase was fixed probably due to vitrification.

CONCLUSIONS

The mixture of Novolac/EVA is miscible over a large composition and temperature range, mainly owing to the intermolecular hydrogen-bonding interaction between carbonyl groups of EVA and phenolic hydroxyl groups of Novolac. Novolac/EVA mixtures show a LCST phase

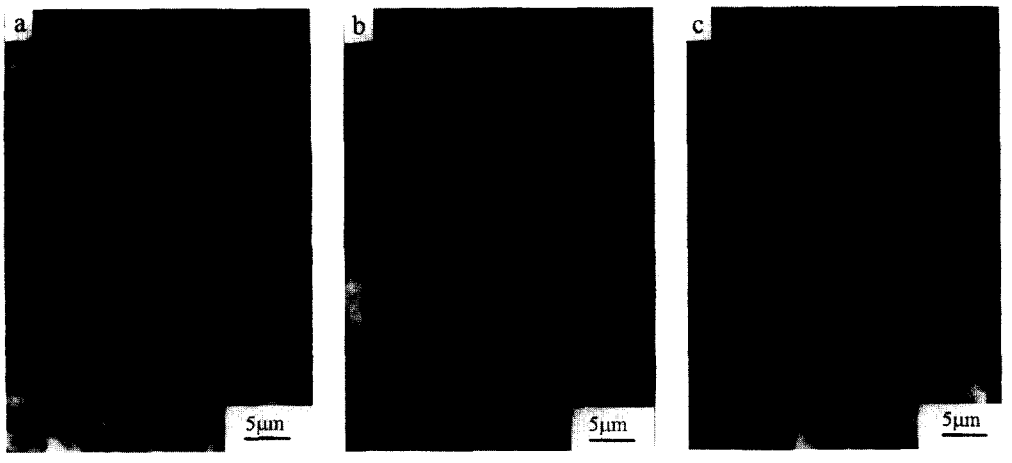

Figure 11 Scanning electron micrographs of fractured surface for 50/50/15 (wt) Novolac/EVA/Hexa mixture cured at 150°C for various times: (a) $t = 20$ min; (b) $t = 40$ min; (c) $t = 60$ min

diagram with high asymmetry; the immiscible region in the phase diagram emerges at high temperature and high Novolac content.

An initially homogeneous Novolac/EVA mixture underwent phase separation via SD during the curing reaction with Hexa as curing agent. The structure formation process can be interpreted in terms of a phase separation scheme based on SD, which is induced by the increase in molecular weight of Novolac in the curing process. A regularly cocontinuous phase-separated structure was yielded ultimately by curing reaction-induced SD. The process of SD during curing reaction is different from that in iso-quench thermally induced SD, i.e. q_m increases with time in the early stage of curing. The scaled structure function analysis and SEM observation show that the final morphology of a fully cured mixture of Novolac/EVA may be yielded through the route of cluster to the cocontinuous structure.

ACKNOWLEDGEMENTS

The authors gratefully acknowledge the financial support of the National Nature Science Foundation of China and 'the Best Younger Teachers' Foundation' of the National Education Commission of China.

REFERENCES

1. See for example: Matsumoto, A., Hasegawa, K., Fukuda, A. and Otsuki, K., *J. Appl. Polym. Sci.*, 1991, **43**, 365; 1992, **44**, 205; 1992, **44**, 1547. Simitzis, J., Karagiannis, K. and Zoumpoulakis, L., *Eur. Polym. J.*, 1996, **32**(7), 857; *Polymer International*, 1995, **38**, 183.
2. Inoue, T., *Prog. Polym. Sci.*, 1995, **20**, 119.
3. Yamanaka, K. and Inoue, T., *Polymer*, 1989, **30**, 662.
4. Yamanak, K., Takagi, Y. and Inoue, T., *Polymer*, 1989, **60**, 1839.
5. Yamanaka, K. and Inoue, T., *J. Mater. Sci.*, 1990, **25**, 241.
6. Chen, W., Kobayashi, S., Inoue, T., Ohnaga, T. and Ougizawa, T., *Polymer*, 1994, **25**, 4015.
7. Nakamura, G., Kim, B. and Inoue, T., *Polym. Prep. Jpn.*, 1990, **39**, 3557.
8. Coleman, M. M., Serman, C. J. and Painter, P. C., *Macromolecules*, 1987, **20**, 226.
9. Zhang, X. and Solomon, D. H., *Macromolecules*, 1994, **27**, 4919.
10. Hashimoto, T., Sasaki, K. and Kawai, H., *Macromolecules*, 1984, **17**, 2812.
11. Moskala, E. J., Howe, S. E., Painter, P. C. and Coleman, M. M., *Macromolecules*, 1984, **17**, 1671.
12. Serman, C., Painter, P. and Coleman, M., *Polymer*, 1991, **32**, 1049.
13. He, M., Liu, Y., Feng, Y., Jiang, M. and Han, C., *Macromolecules*, 1991, **24**, 464.
14. Bhagwagar, D., Painter, P. and Coleman, M., *Macromolecules*, 1994, **27**, 7139.
15. Hashimoto, T., Kumaki, J. and Kawai, H., *Macromolecules*, 1983, **16**, 641.
16. Cahn, J., *J. Chem. Phys.*, 1965, **42**(1), 93.
17. See for example: Furukawa, H., *Adv. Phys.*, 1983, **79**, 6387. Binder, K. and Stauffer, D., *Phys. Rev. Lett.*, 1974, **33**, 1006. Lifshitz, I. M. and Slyozov, V. V. *J. Phys. Chem. Solids*, 1961, **19**, 35.
18. Ohnaga, T., Chen, W. and Inoue, T., *Polymer*, 1994, **35**, 3774.
19. Hashimoto, T., Itakura, M. and Hasegawa, H., *J. Chem. Phys.*, 1986, **85**(10), 6118.
20. Furukawa, H., *Physica (A)*, 1984, **123**, 497.
21. Okada, M., Fujimoto, K. and Nose, T., *Macromolecules*, 1995, **28**, 1795.